Dissipation signatures of the normal and superfluid phases in torsion pendulum experiments with ^{3}He in aerogel

N. Zhelev,[1] R. G. Bennett,[1] E. N. Smith,[1] J. Pollanen,[2] W. P. Halperin,[2] and J. M. Parpia[1]

[1]*Laboratory of Atomic & Solid State Physics, Cornell University, Ithaca, New York, 14853 USA*

[2]*Department of Physics and Astronomy, Northwestern University, Evanston, Illinois 60208, USA*

We present data for the energy dissipation factor Q^{-1} over a broad temperature range at various pressures of a torsion pendulum setup used to study ^{3}He confined in a 98% open silica aerogel. Values for Q^{-1} above T_c are temperature independent and have weak pressure dependence. Below T_c, a deliberate axial compression of the aerogel by 10% widens the range of metastability for a superfluid equal spin pairing (ESP) state; we observe this ESP phase on cooling and the B phase on warming over an extended temperature region. While the dissipation for the B phase tends to zero as T $\rightarrow$ 0, Q^{-1} exhibits a peak value greater than that at T_c at intermediate temperatures. Values for Q^{-1} in the ESP phase are consistently higher than in the B phase and are proportional to ρ_s/ρ until the ESP to B phase transition is attained. We apply a viscoelastic collision-drag model, which couples the motion of the helium and the aerogel through a frictional relaxation time τ_f. We conclude that unless τ_f is an order of magnitude larger than expected, an additional mechanism to dissipate energy not captured in the collision-drag model and related to the emergence of the superfluid order must exist. The extra dissipation below T_c is possibly associated with mutual friction between the superfluid phases and the clamped normal fluid. The pressure dependence of the measured dissipation in both superfluid phases is likely related to the pressure dependence of the gap structure of the "dirty" superfluid. The large dissipation in the ESP state is consistent with the phase being the A or the Polar with the order parameter nodes oriented in the plane of the cell and perpendicular to the aerogel anisotropy axis.

I. INTRODUCTION

Unconventionally paired Fermi systems exhibit strong sensitivity in their transport properties to the presence of even a small degree of nonmagnetic impurities [1–6]. For the otherwise pure superfluid ^{3}He, an elastic scattering mechanism, in addition to the inelastic two-particle scattering processes, is provided by porous silica aerogel "impurities" [7–10]. Since the discovery of superfluidity of ^{3}He in aerogel [11,12], the analogy of this so-called "dirty" Fermi superfluid with "dirty" unconventional superconductors has been investigated in the literature. Transport measurements in the normal Fermi liquid (spin [13,14], thermal conductivity [15,16], and viscosity [17]) reveal a crossover from an intrinsic inelastic quasiparticle-quasiparticle (qp-qp) scattering rate at high temperatures to a quasiparticle-impurity dominated relaxation mechanism when the temperature is lowered.

In the ^{3}He-aerogel composite system, the ^{3}He is always on the order of the zero-temperature coherence length away from the aerogel strands. The zero-temperature coherence length is defined to be $\xi_0 = \hbar v_F / 2\pi k_B T_c$. It is expected that the superfluid order parameter is suppressed and surface bound states exist near macroscopic surfaces and domain walls [18–20]. However, the aerogel strands do not act as conventional surfaces—else superfluidity would be entirely suppressed. Instead, scattering from the aerogel leads to a suppression of the superfluid gap. We expect a spectrum of low energy excitations inside the gap to appear, which could lead to a gapless superfluid state in which the density of states is finite around the entire Fermi surface [9]. Evidence for such states exists in thermal conductivity [21] and heat capacity [22] measurements as $T \rightarrow 0$, but the exact profile for the density of states of the ^{3}He in aerogel system and its dependence on strong coupling effects is still not fully understood.

In order to probe the dynamics of the aerogel embedded fluid, we have placed the experimental cell in the head of a torsion pendulum. We track the frequency and the quality factor (Q) of the pendulum as the temperature is changed. Observing the frequency shift has proved instrumental in studying the effects of disorder at the onset of superfluid transition [11,23]. However, due to the close spacing between the aerogel strands (of the order of 50 nm), even the small impurity limited viscosity of the normal state ^{3}He would be sufficient to clamp the fluid at the audio frequencies (2.1 kHz) corresponding to the torsional resonant mode we employ. In order to probe the transport properties, we cannot rely on the frequency shift data alone. Instead, in this paper, we focus on the energy dissipation factor (Q^{-1}) of the pendulum, which should be sensitive to the Fermi surface excitations discussed in the previous paragraph.

The aerogel sample is deliberately compressed along the pendulum axis by 10%. It is generally accepted that the aerogel anisotropy due to the axial compression should favor the anisotropic, equal spin pairing (ESP) superfluid ^{3}He-A phase [24,25]. Previously, we would have also expected that the ℓ vector would preferentially align along the axis of compression. However, recent pulsed NMR tip angle measurements on axially compressed aerogel at moderate magnetic fields (both along and perpendicular to the strain axis) show that the ℓ vector tends to be oriented in the plane of the cell and perpendicular to the strain axis regardless of the direction of the magnetic field [26]. Recent theoretical results [27] also point to the possibility of a Polar phase (also an ESP phase) with a line of nodes away from the strain axis. In an earlier work, we observed that the superfluid fraction in the ESP phase is less than that in the B phase [23]. If ℓ in the A phase (nodal direction in the Polar phase) was

aligned perpendicular to the flow, we would instead observe the superfluid fraction in the A phase exceeding that in the B phase [28,29]. Thus consistent with the equal spin pairing state realized in this experiment is either an A phase with ℓ randomly oriented along the plane of the cell or a Polar phase. Lacking NMR data to identify the phase at zero magnetic field, we refer to the intervening phase as ESP rather than the A/Polar phase.

The metastable ESP phase is supercooled to temperatures well below the equilibrium ESP to B phase boundary. On the other hand, after completion of the ESP to B transition by further cooling the cell, the superfluid B phase persists on warming and the ESP phase only reappears in a region of small temperature width very close to T_c. This results in a significant range of temperatures over which we have ESP phase on cooling and B phase on warming, and allows us to make a direct comparison of the properties (ρ_s, Q^{-1}) of the two superfluid phases.

In the following sections, we briefly outline experimental details, and present the experimental data. Then we discuss a model for the energy dissipation factor of the torsion pendulum arising from the normal state fluid. Finally, we discuss the data below T_c, where we observe additional dissipation intrinsic to the superfluid. We relate our data to the presented theoretical model and propose a possible mechanism that could account for the observed behavior.

II. EXPERIMENTAL SETUP

A. Construction of the torsion pendulum

The torsion pendulum consisted of two hollow beryllium-copper torsion rods: an upper one with a 1.27-mm outer diameter, and a lower one with an outer diameter of 1.22 mm. A 1-mm diameter hole, bored through both torsion rods, served as a fill line for the fluid into the pendulum's head. An epoxy joint coupled the pendulum "head" to the upper torsion rod.

Two magnesium "wings," electrically insulated from the rest of the pendulum, were attached to the cylindrical mass at the junction of the two torsion rods. Each of the wings was maintained at 100-V bias with respect to closely spaced adjacent electrodes. A function generator was connected to one of the electrodes to drive the pendulum capacitively. The resulting motion of the pendulum induced a small ac voltage in the second electrode, which was amplified and sensed by a dual phase lock-in amplifier.

The pendulum can be excited at two torsion resonance modes: a symmetric mode in which the wings and the head of the pendulum move in phase, and an antisymmetric mode when they move out of phase. The latter mode provides greater sensitivity to motion of the fluid in the head and lower noise and was thus selected for this experiment.

The 98% open silica aerogel was grown directly into a pillbox shaped stainless steel cavity consisting of a tightly fitted lid, a base and a shim inserted between them. More information about the physical properties and method of growth of aerogel can be found in Ref. [30].

The aerogel was compressed by 10% along its main axis by removing the shim and pressing the lid onto the base, bringing the height of the cell to 400 μm. The height was chosen to be
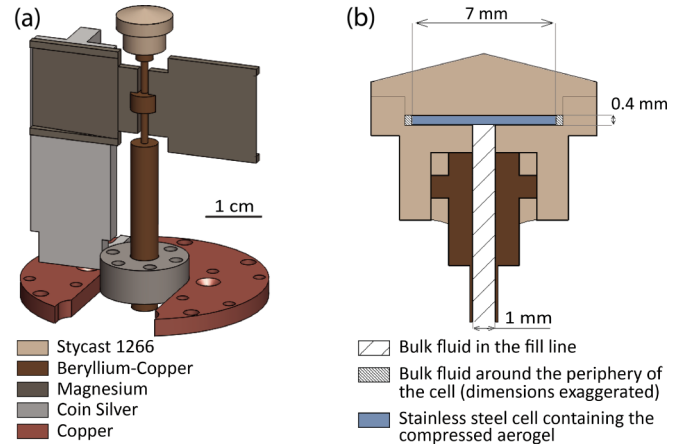

FIG. 1. (Color online) (a) A schematic for the torsion pendulum setup. (b) A cross-section of the torsion pendulum head. The cell in which the aerogel was grown and compressed is shown with its dimensions. Indicated are also the regions of bulk fluid in the cell. Note that the gap between the cell and the epoxy cast around the cell's periphery is greatly exaggerated.

small enough to couple the aerogel well to the walls (though aerogel displacement relative to the walls of the cell still needs to be considered), but large enough to ensure fine resolution in determining the fraction of superfluid. The moment of inertia of the torsion head and aerogel filled cell is calculated to be 0.064 g cm^2 and that of the helium at saturated vapor pressure -5.85×10^{-5} g cm^2, or about 1 part in 10^3 of the inertia of the head.

The steel cavity was dry fitted into an already hardened epoxy cast in order to reduce possible contamination of the aerogel by any epoxy penetrating through holes in the stainless pillbox. Despite careful machining of the epoxy cast, there appeared to be empty regions around the periphery of the cell occupied by ^{3}He not embedded in the aerogel (bulk fluid). In addition, we need to consider the bulk fluid within the fill line inside the upper torsion rod in our subsequent analysis. Appendix A describes how we modeled the contribution coming from these two regions.

A schematic of the torsion pendulum setup along with a detailed sketch of the head of the pendulum is shown at Fig. 1. The locations of the inferred bulk fluid regions are also indicated.

B. Thermometry and data acquisition

Thermometry was provided through a ^{3}He melting curve thermometer (MCT), which had $a \sim 30$ min (dependent on the temperature) time constant with respect to the ^{3}He in the aerogel. A quartz tuning fork immersed in the ^{3}He fluid allowed for a more immediate reading of the temperature of the ^{3}He in the torsion head. The fork was swept through resonance every ten minutes, and its frequency and quality factor recorded. These values were calibrated against the MCT and provide secondary thermometry for the experiment.

After acquiring the resonance curve at a fixed temperature (T_0), we fitted the resonance and established the quality factor at this temperature $Q(T_0)$. We also plotted the values of the

quadrature (Y) and in-phase (X) components of the signal against each other. They formed a circle with a diameter equal to the signal amplitude at resonance (A), centered at ($A/2, 0$). Provided that we drove the pendulum within ± 0.1 radian of phase error with respect to resonance, we could deduce the resonant frequency and Q of the pendulum using the following relationships:

$$f_{\rm res}(T) = f_{\rm drive}(T) \left[1 + \frac{Y(T)}{2Q(T)X(T)} \right], \qquad (1)$$

$$Q(T) = \frac{V_{\rm drive}(T_0)}{V_{\rm drive}(T)} \frac{Q(T_0)}{A(T_0)} \frac{X^2(T) + Y^2(T)}{2X(T)}, \qquad (2)$$

where $Q(T_0)$, $A(T_0)$ were determined from the sweep. To avoid driving the pendulum at a level away from its linear behavior, the driving amplitude was also adjusted when it deviated more than 3% from its target value. The amplitude of motion of the pendulum's wings was of the order of a few angstroms leading to a peak velocity of about a few μm/s. The typical noise in data obtained in this manner was 2.5×10^{-9} for the inferred resonant frequency and 2.5×10^{-3} for the quality factor.

The additional energy dissipated by the fluid is determined by subtracting the empty cell value for $Q^{-1}(T)$ from the values of $Q^{-1}(T)$ when filled with ^{3}He. The superfluid fraction of the fluid [ρ_s/ρ (P,T)] can be found through the relative reduction in the moment of inertia of the torsion pendulum head as the temperature is lowered below T_c for the fluid in the aerogel. From knowledge of the period [$p(P,T) = f_{\rm res}^{-1}(P,T)$] of the torsion pendulum when the fluid is fully locked to it [$p_0(P)$] and the period when the cell is empty ($p_{\rm empty}$), we can define the superfluid fraction as ρ_s/ρ (P,T) = [$p_0(P) - p(P,T)$]/[$p_0(P) - p_{\rm empty}$].

To map the temperature dependence of the empty cell values for the period and dissipation, we took points at discrete temperatures between 100 and 1 mK, waiting for a few hours to reach equilibrium between points, before any ^{3}He was

introduced in the cell. Plots for the empty cell data can be found in Ref. [31]. Both the pendulum's period and the quality factor change very little below 5 mK. We attribute this to the time dependent heat release from the epoxy [32]. By plotting the data versus $\log_{10}(T)$, we extrapolate the empty cell data below 5 mK. We assign the uncertainty for Q^{-1} in the empty cell to be $\sim 1 \times 10^{-6}$. The relative uncertainty in the empty cell period below 5 mK is also estimated to be $\sim 1 \times 10^{-6}$, or 1 part in 1000 of ($p_0 - p_{\rm empty}$).

Near T_c, the viscosity of bulk normal ^{3}He ensures that even at high pressures, the ^{3}He is well locked to any cavities smaller in size than ~ 100 μm at kilohertz frequencies. Thus the period of the pendulum at T_c would be $p_0(P)$ apart from a correction due to the fluid in the fill line, which can be accurately calculated (see Appendix A).

III. DATA

A. Normal state

Figure 2 summarizes the data for the energy dissipation factor due to ^{3}He fluid versus temperature in the normal state at four widely spaced pressures: 0.14, 2.6, 15.7, and 25.7 bar. In each of these measurements, we changed the temperature in discrete steps and waited until the signal for the frequency and Q of the pendulum reached equilibrium. The wait time varied with temperature and was of order two hours or less. The calculated dissipation from the bulk fluid regions is shown as solid and broken lines. Subtracting this contribution from the data taken in the normal state, we observe a residual dissipation of $\sim (2.4 \pm 0.6) \times 10^{-6}$ that we attribute to the ^{3}He liquid in the aerogel. The uncertainty arises mainly from the need to infer the geometries of the bulk fluid regions. It is important to note that the dissipation does not have an obvious temperature dependence and any pressure dependence cannot be discerned from the plot in Fig. 2.
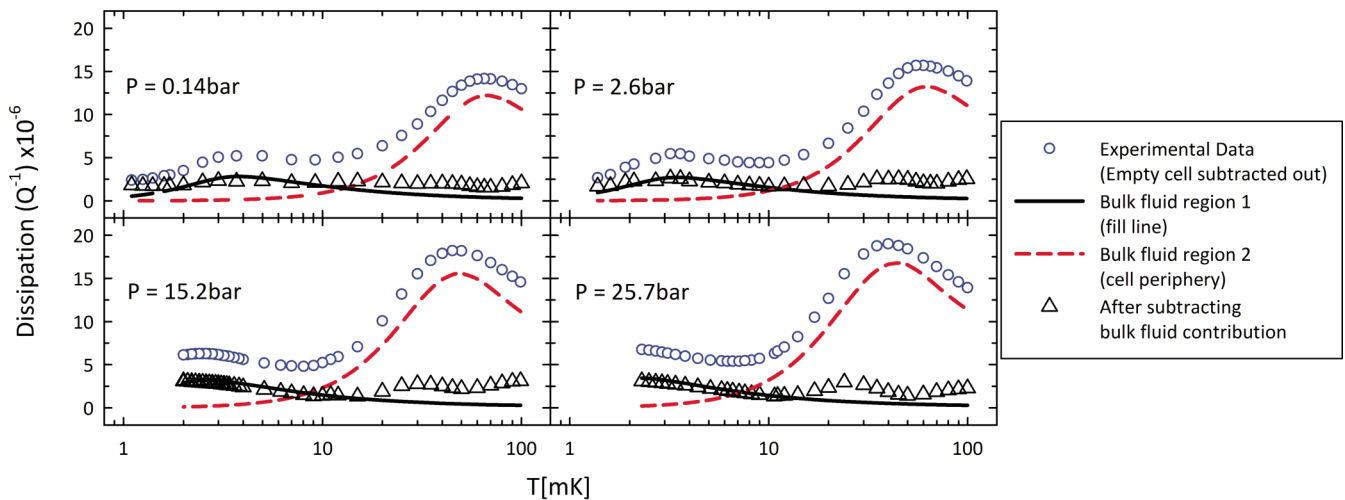

FIG. 2. (Color online) Experimental data for Q^{-1} vs temperature for four pressures after empty cell data are subtracted (open (blue) circles). Shown also are the fits for the bulk fluid contribution to the Q^{-1} for two components: bulk fluid contained in the fill line [solid (black) line] and the bulk fluid around the periphery of the cell, modeled as a channel of thickness 28 μm [dashed (red) line]. After subtracting off the two bulk fluid contributions, the dissipation due to the ^{3}He and aerogel combination is shown as the open (black) triangles. The dissipation of $\sim 2.4 \times 10^{-6}$ is essentially temperature and pressure independent within the scatter in the normal state data ($\sim \pm 0.6 \times 10^{-6}$).
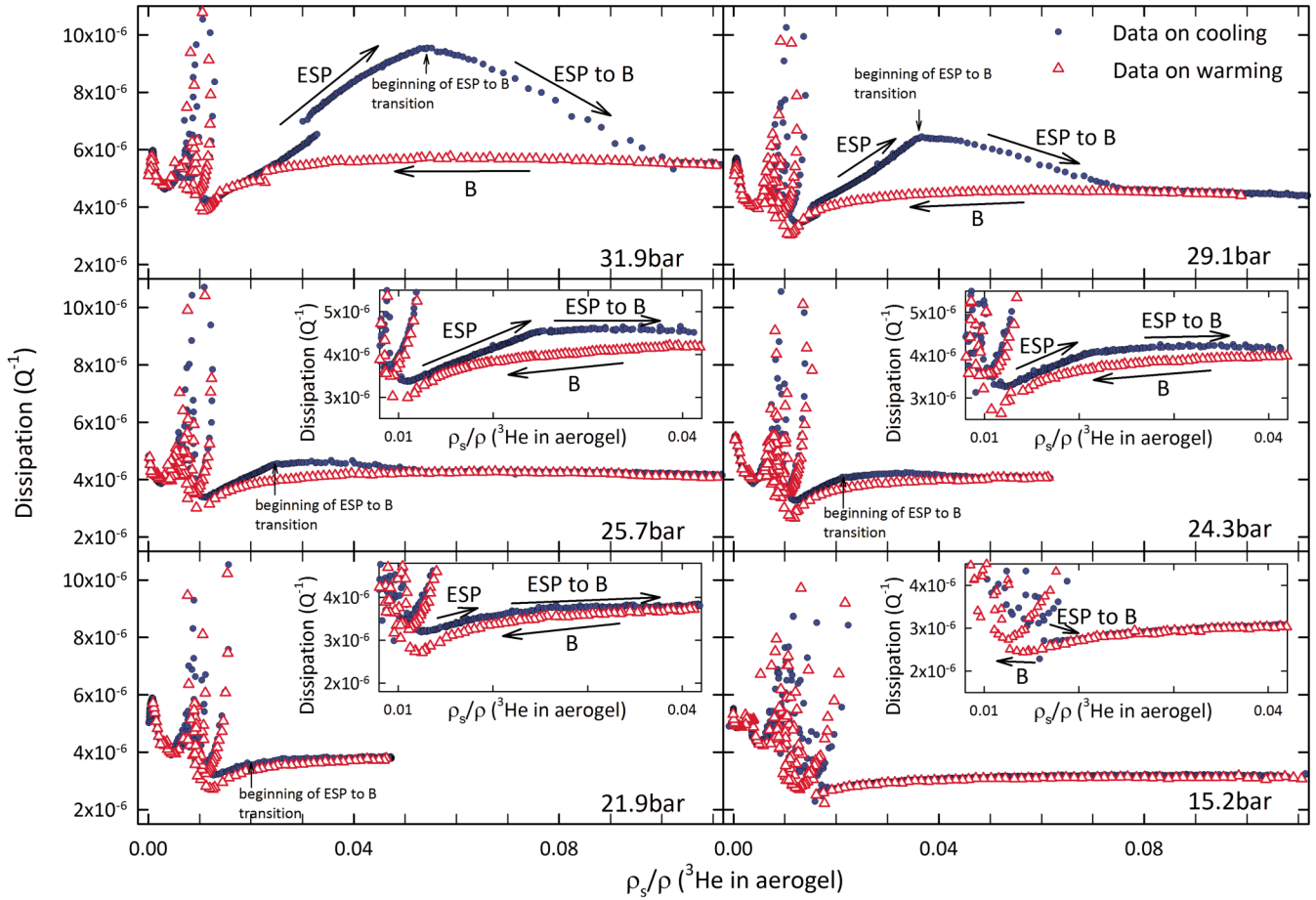
FIG. 3. (Color online) Data for Q^{-1} vs ρ_s/ρ at six different pressures are plotted. We note slow mode resonance crossings for $\rho_s/\rho < 0.015$. ESP-phase (cooling-blue solid circles) and B-phase (warming-red open triangles) coexistence regions are shown in the insets at lower pressures. The dissipation is larger in the ESP-phase compared to the B phase. The higher dissipation associated with the ESP phase is especially evident at higher pressures and close to the ESP to B transition. Bulk fluid contributions have been subtracted, assuming bulk B phase. The discontinuity in the 31.9-bar data on cooling is due to the bulk A to B transition.

B. Superfluid state of ^{3}He in aerogel

Data were taken on both cooling and warming in the superfluid state at a number of different pressures, maintaining a constant cooling (warming) rate ($\sim$30 μK/hr). From knowledge of the bulk superfluid fraction and viscosity, we subtracted contributions due to the bulk regions in order to determine the corresponding values for the ^{3}He in the aerogel. In particular, we note that bulk fluid Q^{-1} is at most $\sim$4 $\times$ 10^{-6} near T_c and rapidly decreases at lower temperatures, and is thus unable to account for the measured dissipation. A summary of the data for Q^{-1} versus $(\rho_s/\rho)_{\text{aerogel}}$ at six different pressures is shown in Fig. 3.

Standing wave modes of the fourth-sound like "slow mode" (in which the superfluid moves out of phase with the normal fluid; normal fluid is clamped to the nonrigid aerogel) cross the torsional oscillator frequency, as the slow mode's velocity evolves, between $0 \leqslant (\rho_s/\rho)_{\text{aerogel}} \leqslant 0.015$. We can identify the resonance crossings in Fig. 3 as a number of closely spaced "loops." These resonance effects [33–37] will be ignored in our subsequent discussions.

The superfluid transition temperatures and precise phase diagram for this sample were identified in our previous publication [23]. Below the superfluid transition, we enter the

superfluid ESP phase on cooling. At lower temperatures, we observe a continuous phase transition between the ESP and the B phases (extended over a temperature interval of $\sim$70 μK). It is thought that this width is due to the strong pinning of the phase interface by the aerogel. On warming, we stay in the B phase until just below the critical temperature. The reappearance of the ESP phase is very pressure dependent. This strongly hysteretic behavior allows us to probe ESP and B phase properties over an extended temperature window, especially at elevated pressures.

The pressure dependence of Q^{-1} against $(\rho_s/\rho)_{\text{aerogel}}$ and $(1 - T/T_c)$ is shown in Fig. 4. In the B phase, we observe a broad peak in the dissipation [Fig. 4(a)]. Below T_c the dissipation rises, even though the impurity limited normal fluid viscosity should be constant. The dissipation in the ESP phase rises even faster than in the B phase [Fig. 4(b)]. This is in sharp contrast with experiments in the bulk, where the viscosity is seen to drop sharply below T_c and scale as $e^{-\Delta/k_B T}$ in the finite size regime [38]. $Q^{-1}(T)$ scales well with ρ_s/ρ and not $(1 - T/T_c)$, as shown in Figs. 4(a) and 4(c). Since $\rho_s/\rho \propto \Delta^2$, this implies that Q^{-1} and the energy gap Δ are related. The anomalous dissipation of the ESP phase scales almost linearly with ρ_s/ρ [Fig. 4(b)], and exceeds the corresponding
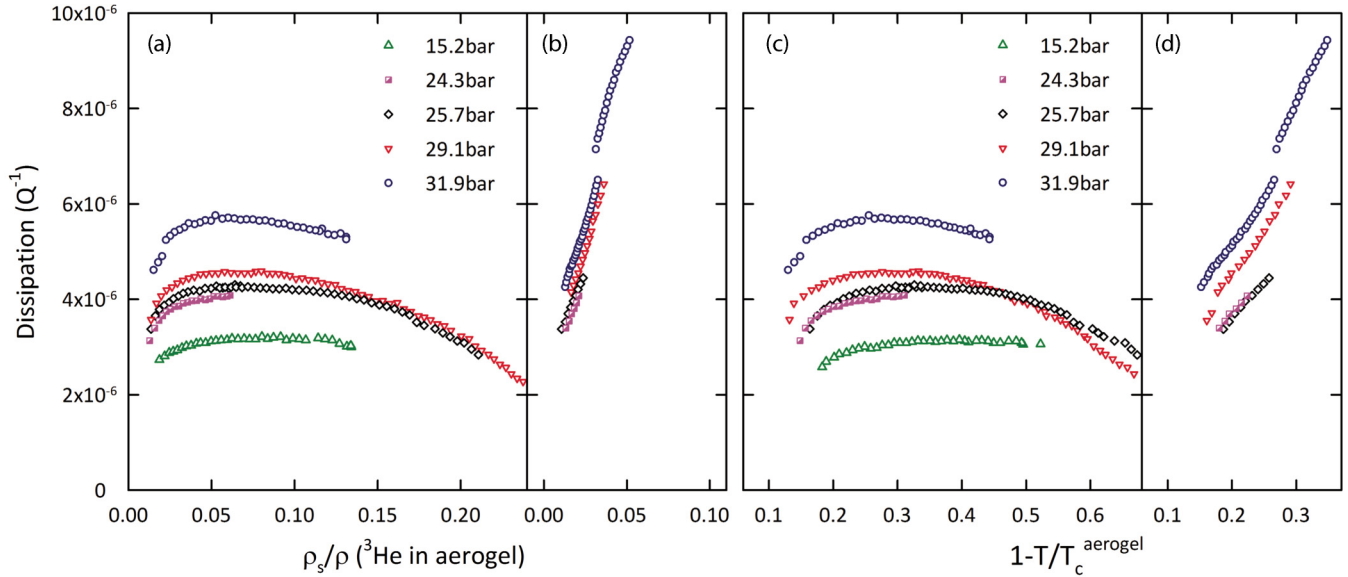
FIG. 4. (Color online) (a) A plot of Q^{-1} in the B phase vs ρ_s/ρ for all the data sets in Fig. 3 combined in one plot. We note the consistent pressure dependence of Q^{-1} with ρ_s/ρ. Strong coupling effects enhance the anomalous superfluid dissipation. (b) A plot of Q^{-1} in the ESP phase vs ρ_s/ρ for all the data. The pressure dependence of Q^{-1} is seen to arise mainly due to the larger extent in temperature of the ESP phase at high pressure; the Q^{-1} scales well with ρ_s/ρ. Discontinuities in the data are due to the bulk A $\rightarrow$ B transition on cooling. (c) and (d) Plots of Q^{-1} vs $1 - T/T_c^{\text{aerogel}}$ in the B and ESP phases, respectively. Much of the scaling behavior is lost in this view compared to that seen in (a) and (b).

value of Q^{-1} at the same ρ_s/ρ (and T/T_c) in the B phase. As pressure is increased, Q^{-1} measured in the ESP phase rises considerably above the values for Q^{-1} in the B phase. This effect is emphasized further since the width of temperature region in which the ESP phase is stable on cooling increases with pressure.

IV. COMPARISON TO EXPERIMENTS WITH UNCOMPRESSED AEROGEL

Previous torsion pendulum experiments with uncompressed aerogel [11,39] used significantly larger aerogel samples and had much lower Q's. Thus no direct comparison with previous torsion pendulum experiments can be made. However, we can relate the Q^{-1} reported here (in the superfluid state) to the Q of the slow mode of ^{3}He in uncompressed aerogel samples in the ESP (Ref. [40]) and the B (Ref. [41]) phases . Results for the B-phase ultrasound dissipation can also be found in Ref. [55]. The qualitative behaviors described in these references (increased ESP- and B-phase dissipation as the temperature is lowered near T_c, $Q_{\text{ESP}}^{-1} > Q_B^{-1}$) are similar to what we observe. Thus apart from allowing the ESP state to persist on cooling to much lower temperatures, the aerogel compression is probably not a significant factor in the observed results.

V. COLLISION DRAG MODEL IN A TORSION PENDULUM GEOMETRY

A starting point in the model for the dynamics of the helium-aerogel system is to map out the angular velocity profiles of the fluid and the aerogel across the flow channel. We expect the fluid to be in a Drude flow regime [10,17], where the

angular velocity of the fluid with respect to the aerogel is constant across the channel, with the exception of a small region of size $\delta_d = \sqrt{(\eta\tau_f/\rho)}$ away from the edges [17,41]. The frictional relaxation time τ_f is related to the friction force per unit volume coupling the helium with the aerogel matrix [42–44]:

$$\mathbf{F}(\mathbf{v_l},\mathbf{v_a}) = \frac{\rho}{\tau_f}(\mathbf{v_l} - \mathbf{v_a}), \tag{3}$$

where $\mathbf{v_l}$ and $\mathbf{v_a}$ are, respectively, the velocities of the normal ^{3}He and the aerogel. The frictional force can be related to the average change of momentum a quasiparticle experiences upon scattering from an aerogel impurity.

In Ref. [44], τ_f is given by

$$\tau_f = \frac{\tilde{\tau}}{\left(1 - \frac{\rho_s^0}{\rho}\right)\left[1 + \frac{F_s^1}{3}\left(1 - \frac{\rho_s^0}{\rho}\right)\right]} \tag{4}$$

with F_s^1 being a Landau parameter. The bare superfluid density, ρ_s^0 is related to the measured superfluid density stripped of Fermi-liquid effects through:

$$1 - \frac{\rho_s}{\rho} = \frac{m^*}{m}\frac{1 - \frac{\rho_s^0}{\rho}}{1 + F_s^1\left(1 - \frac{\rho_s^0}{\rho}\right)}. \tag{5}$$

In the normal state, $\tilde{\tau}$ is the transport relaxation time equal to the quasiparticle mean free path divided by the Fermi velocity [45]. In the superfluid state, however, $\tilde{\tau}$ is temperature dependent. Reference [44] defines $\tilde{\tau}$ in terms of integrals of quasiclassical Keldysh Green's functions, but no direct relationship between $\tilde{\tau}$ and conventional experimental observables in the superfluid state is shown. Instead, the values for $\tilde{\tau}$ are numerically calculated in the different scattering

limits for various degrees of T_c suppression by the aerogel. It is evident from the plots for $\tilde{\tau}(T)$ given in in Ref. [44] that $\tilde{\tau}$ in the superfluid state could be somewhat larger that $\tilde{\tau}$ in the normal state, before $\tilde{\tau}(T)$ eventually approaches zero as $T \to 0$.

The quasiparticle mean free path can be estimated from the suppression of the superfluid transition as discussed in Ref. [23] using a model proposed by Abrikosov and Gorkov in Ref. [46] and refined into the isotropic inhomogeneous scattering model (IISM) described in Refs. [7,47–49]. Assuming a Fermi velocity of 30 m/s, the value of the normal state τ_f inferred from the 155-nm mean free path used to fit the T_c suppression is $\approx 5 \times 10^{-9}$ s.

The sound velocity in the aerogel sample is expected to be in the range of $c \sim 30$–50 m/s [33,50]. For a frequency of 2.1 kHz, we expect a compressional sound mode wavelength of a few millimeters, an order of magnitude larger than the height of the cell. Yet, there will be a small displacement of the aerogel in the interior of the cell relative to the motion of the adjacent wall. The normal helium is well locked to the aerogel; the aerogel and helium form a composite medium exhibiting a velocity profile largely determined by the viscoelasticity of the aerogel. Through numerical calculations, we predict $a \sim 1\%$ difference in the angular velocity in the middle of the cell and the wall. This angular velocity profile gives rise to dissipation in the cell. In addition, there is a small velocity difference between the entrained fluid and the aerogel itself that arises due to the finite value of τ_f.

To solve for the angular velocity profiles of the helium and the aerogel, we write the Navier-Stokes and wave equations, coupled by the collision drag force:

$$\rho \dot{\Omega}_l = \eta \frac{\partial^2 \Omega_l}{\partial z^2} - \frac{\rho}{\tau_f}(\Omega_l - \Omega_a), \tag{6}$$

$$\rho_a \dot{\Omega}_a = i \frac{\mu}{\omega} \frac{\partial^2 \Omega_a}{\partial z^2} + \frac{\rho}{\tau_f}(\Omega_l - \Omega_a), \tag{7}$$

where $\Omega_l(z)$ and $\Omega_a(z)$ are the angular velocity profiles of the helium liquid and the aerogel across the channel, respectively. The shear modulus of the aerogel is μ, which we can deduce from the aerogel sound velocity. The viscosity of the helium η equal to that of the bulk liquid at high temperatures, but reaches an impurity limited value at about 10 mK, leading to $\eta \lesssim 0.01$ Poise.

Having solved for the angular velocity profiles, we find the induced torque on the walls of the cell due to the motion of the helium liquid (N_l) and the aerogel (N_a). With the assumption that the angular velocities of the liquid and the aerogel at the walls are equal to the angular velocity of the cell wall, i.e., $\Omega_{l(a)}(\pm z/2) = \dot{\theta}$, we obtain

$$N_l = -\pi R^4 \eta \left(\frac{\partial \Omega_l}{\partial z} \right)_{z=h/2}, \; N_a = -i\pi R^4 \frac{\mu}{\omega} \left(\frac{\partial \Omega_a}{\partial z} \right)_{z=h/2}.$$

The empty cell Q^{-1} shows a nonzero value when extrapolated to $T = 0$. Yet, a purely elastic aerogel should not be dissipative. A previous iteration of this experiment used an aerogel sample (grown in a different process) with a height of ≈ 4 mm. The otherwise identical torsion pendulum containing that sample had a $Q \approx 100\times$ lower than the one described

here. We can expect a h^2 dependence of the dissipation, with h being the height of the cell. Furthermore, there have been a number of experiments on silica aerogels (though on samples denser compared to ours and at room temperature [51–53]), that report a complex elastic modulus, which would lead to dissipation effects associated with the plastic deformations of the aerogel. We write the shear modulus of the aerogel as $\mu = \mu_{\text{re}} - i \mu_{\text{im}}$.

Accounting for the complex shear modulus, we obtain

$$
\begin{aligned}
Q^{-1}(T) &= -\frac{\text{Re}(N_a + N_l)}{I_0 \omega \dot{\theta}} \\
&\approx \frac{I_a}{I_0} \left[1 + \frac{\rho_n(T)}{\rho} \frac{\rho}{\rho_a} \right]^2 \frac{\rho_a \omega^3 h^2}{12 \mu_{\text{re}}^2} \left[\eta(T) + \frac{\mu_{\text{im}}}{\omega} \right] \\
&\quad + \frac{\rho_n(T)}{\rho} \frac{I_l}{I_0} \omega \tau_f.
\end{aligned} \tag{8}
$$

More details about the exact solution to the equations of motion and how we derive the result for Q^{-1} can be found in Appendix B.

VI. DISCUSSION

There are three terms in Eq. (8) that contribute to the normal state dissipation. The first one is proportional to the normal fluid viscosity $\eta(T)$ and is due to the aerogel flexure modifying the angular velocity profile of the liquid and causing extra dissipation. Using $\eta \sim 0.01$ Poise, this term accounts for a contribution to Q^{-1} of the order of $\sim 10^{-8}$. In order to match the experimental value of $Q^{-1} = 2.4 \times 10^{-6}$, we need η to be two orders of magnitude larger, which we consider unphysical.

The third term in Eq. (8) contains contributions to Q^{-1} arising from the frictional relaxation time τ_f. For this term to have a large enough contribution to match the experimental data for Q^{-1}, we need $\tau_f \sim 10^{-7}$ s. However, the quasiparticle mean free path in a 98% open aerogel has been shown to be $\lesssim 200$ nm [13,15,21–23,54]. Assuming a Fermi velocity of 30 m/s and effective mass $m^*/m \sim 3$–5, we find that τ_f above T_c can at most be a few nanoseconds.

We suggest that the large temperature independent normal state dissipation could be due to the intrinsic dissipative nature of the aerogel, characterized by the ratio $\mu_{\text{im}}/\mu_{\text{re}}^2$. The reason we are sensitive to the aerogel intrinsic dissipation term is the low-resonant frequency of the torsion pendulum. Since this term depends on μ_{im}/ω [Eq. (8)], its contribution would be less significant at the higher frequencies employed in ultrasound attenuation experiments [17,55]. To obtain Q^{-1} of the order of 10^{-6}, we need $\mu_{\text{im}}/\mu_{\text{re}} \sim 0.1$. Such a large loss tangent could be due to the fractal nature of the aerogel or could be related to the expected presence of a few monolayers of solid ^{3}He on the surface of the aerogel strands.

Figure 5 shows the pressure dependent values for Q^{-1} at T_c^{bulk} with the contributions from bulk fluid and the empty cell subtracted plotted versus $[1 + \rho(P, T_c^{\text{bulk}})/\rho_a]^2 - 1$ [see Eq. (8)]. The transition temperature as a function of pressure is well known as are the density and the viscosity of the bulk fluid at T_c allowing us to accurately subtract the bulk fluid contributions and reveal the pressure dependence of Q^{-1} in the normal state. If our assumption that the main contribution
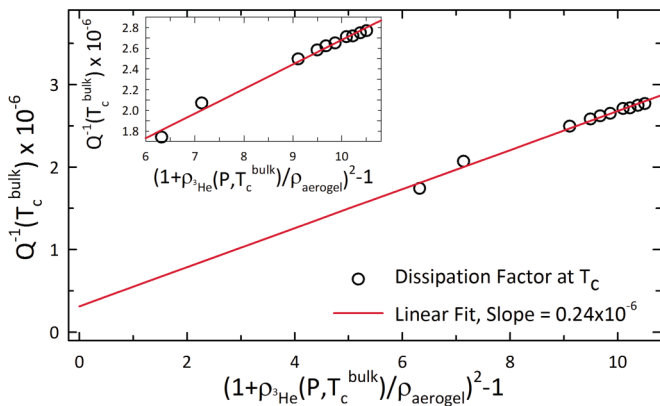
FIG. 5. (Color online) A plot of Q^{-1} measured at T_c for 0.14, 3, 15.2, 18.5, 20.1, 21.9, 24.3, 25.7, 27.5, and 29.1 bar (pressure increases as we go from left to right) with the bulk fluid and empty cell dissipation subtracted versus $(1 + \rho_s/\rho_{aerogel})^2 - 1$. A linear regression line is shown, with a slope of $\sim 2.4 \times 10^{-7}$ and y intercept of $\sim 3.1 \times 10^{-7}$.

to the dissipation in the normal state comes from the lossy aerogel, we would expect a linear relationship. A linear fit to the data is shown in Fig. 5, providing an evidence in support of this model. The y intercept of $\sim 3.1 \times 10^{-7}$ could be due to the uncertainty of the empty cell data.

Assuming that energy dissipation of the torsion pendulum due to the interaction of the normal state excitations and the aerogel scales as $[1 + (1 - \frac{\rho_s}{\rho})\frac{\rho}{\rho_a}]^2$, then such a contribution will decrease as the cell is cooled below T_c and deeper in the superfluid state. This cannot explain the dissipation we measure in both the ESP and B phase superfluid states.

We subtract the normal fluid contribution (using parameters from the linear fit in Fig. 5) and consider the residual dissipation. If we allow its origin to be due to the $\frac{\rho_n(T)}{\rho}\frac{I_l}{I_0}\omega\tau_f(T)$ term, we can plot the so-inferred $\tau_f(T)$ as a function of the temperature. Figure 6 shows this for the 29.1-bar data along with the data from Ref. [41]. We find good agreement between the two experiments, implying that the observed dissipation in the 50-kHz sound attenuation experiment and
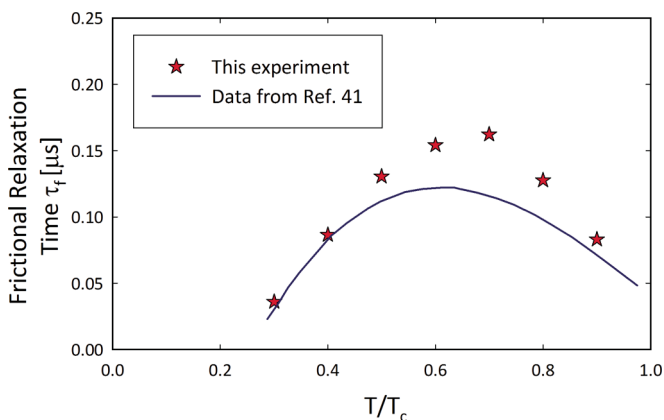

FIG. 6. (Color online) A plot for τ_f as a function of temperature assuming that the τ_f term in Eq. (8) is responsible for all of the extra dissipation we observe in the B phase. The data plotted are for 29.1 bar. We also show the data from Ref. [41], which are deduced in a similar way.

the torsion pendulum Q^{-1} in the superfluid B phase probably have a similar origin. As discussed in the previous section, the relaxation time $\tilde{\tau}$ in Eq. (4) can be shown to increase as we enter the superfluid state due to the rapid opening of the superfluid gap, before $\tilde{\tau}$ eventually diminishes to near zero at extremely low temperatures [44]. In addition, the denominator in Eq. (4) should also decrease as ρ_s/ρ grows. These two effects combined could produce a temperature dependence of τ_f with a similar shape to what we observe in Fig. 6. We can expect an enhancement of τ_f in the superfluid state up to a factor of ten compared to its value at T_c. However, in order to produce a peak τ_f of order 0.15 μs, we need $\tau_f(T_c) \gtrsim 10$ ns, a value which is higher than the few nanoseconds that would be consistent with the T_c suppression measurements. Thus temperature variation of the frictional relaxation time cannot solely produce the observed data. Therefore we conclude that there is an additional mechanism to dissipate energy not captured in the collision-drag model presented in Sec. IV and related to the emergence of the superfluid order.

One way superfluid currents can dissipate energy is through interactions with bound states pinned to the boundary with the normal fluid at the vortex cores [56]. This leads to a mutual friction term, which can be shown to be proportional to [57]

$$\frac{\rho_s}{\rho}\frac{\rho_n}{\rho}(\mathbf{v}_s - \mathbf{v}_n).$$

Such a term would produce a peak in the dissipation similar to what we observe in our data for the B superfluid phase. However, no evidence for vortex states has been found in our experiment. The velocity amplitude of the superfluid current is small, much smaller than the velocities the fluid is driven at in typical experiments observing vorticity [57,58]. We also do not detect a noticeable increase in Q^{-1} as we drive the pendulum harder. While the vortex dynamics model may not be applicable to our experiment, one can imagine that regions of normal fluid with the size of a typical vortex core (coherence length) exist, bound to denser regions of the aerogel. Such bound states will allow for lower energy excitations to interact with the superfluid flow and provide a mechanism for energy dissipation.

An object (in this case an aerogel strand) moving through bulk superfluid with velocity v should feel a force that scales as $e^{-\Delta/k_b T}v$, as shown in Ref. [59]. Assuming that the nodes of the ESP state order parameter tend to orient in the plane of the flow, then we would expect that the ESP state should be associated with higher dissipation than the B phase. However, this argument does not explain the different functional dependence of the dissipation in the ESP phase in terms of ρ_s/ρ compared to the dissipation in the B phase.

Experiments with samples of aerogel attached to vibrating wire resonators immersed in ^{3}He show that flow tends orient the ESP state orbital texture along the flow [60]. Such an effect is clearly demonstrated for velocities significantly larger than the velocities of the fluid in our experiment, but alignment of the ℓ vector is possibly realized also at lower velocities, albeit with a smaller magnitude. Changing the direction of the ℓ vector will damp the flow due to the orbital viscosity of the superfluid [61,62] and manifests itself as the extra dissipation of the pendulum observed in the ESP state. A similar (but smaller) effect has been shown for the B phase if the order parameter is slightly anisotropic [63]. Further, a previous experiment

studying superfluid flow through a small orifice (18-μm diameter) shows large dissipation in the A phase, linearly increases with velocity until a critical velocity is attained [64].

Finally, we note that the pressure dependence of the observed dissipation could be related to the degree of gap suppression in both ESP and B superfluid phases. Dissipation is higher at high pressures, where the gap suppression is less severe, and lower at lower pressures where the superfluid gap tends to be less pronounced and the density of states at lower energies increases.

VII. CONCLUSION

We presented torsion pendulum Q^{-1} data for a compressed aerogel sample filled with ^{3}He in both normal and superfluid states. We developed a model for the normal fluid dynamics as embedded in the viscoelastic aerogel. We assert that frictional relaxation time is not large enough to account for either normal or superfluid Q^{-1} data. Instead, we propose that dissipation features of the data below the superfluid transition originate from the superfluid state.

ACKNOWLEDGMENTS

APPENDIX A: BULK FLUID CONTRIBUTION

We expect the normal state helium liquid to be well locked to the strands of the aerogel. In the normal state, any change in the resonant frequency compared to that of a cell with a fully locked fluid should originate from the bulklike fluid regions of the cell. Figure 7 shows data for the fraction of the moment of inertia not coupled to the walls of the cell at the four experimental pressures that were shown in Fig. 2 (0.14, 2.6, 15.2, and 25.7 bar). The decoupled fluid fraction and dissipation show temperature dependent behavior characteristic of two distinct bulk fluid regions (two peaks in the normal state dissipation data, two "shoulders" in the normal state decoupled fraction data).

The effective length and diameter of the fill line in the torsion rod and the cast epoxy cell are 6 and 1 mm, respectively. The bulk fluid column amounts to 0.8% of the inertia of the fluid in the cell and is designated as bulk fluid region 1. In order to calculate the contribution to dissipation and period shift coming from the fluid in the fill line, we start by calculating the angular velocity profile $\Omega_\theta(r)$ by using the Navier-Stokes equation in a tall cylindrical geometry, which leads to

$$\frac{\partial^2 \Omega}{\partial r^2} + \frac{3}{r}\frac{\partial \Omega}{\partial r} + \frac{i\omega\rho}{\eta}\Omega = 0 \qquad \text{(A1)}$$

with Ω(radius of the cylinder) $= \Omega_{\text{cell}}$.

Solving for Ω we find the torque exerted by the fluid:

$$N = 2\pi R^3 h\eta\left(\frac{\partial \Omega}{\partial r}\right)_{r=R} = \beta_1 + i\omega\beta_2, \qquad \text{(A2)}$$
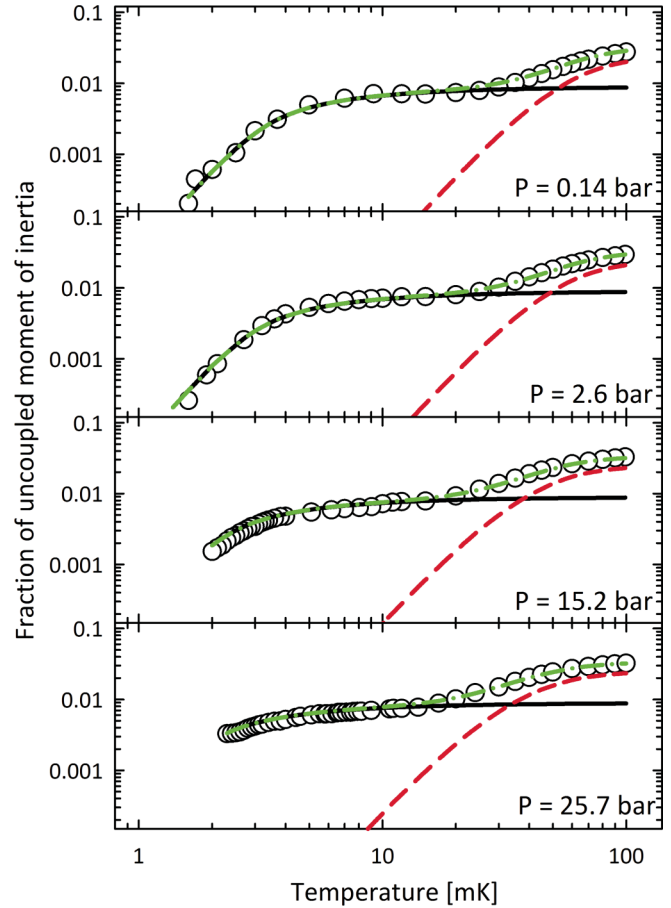

FIG. 7. (Color online) The fraction of fluid decoupled from the pendulum vs temperature for four pressures after background subtraction (open circles). Also shown are the fits for the bulk fluid contribution for two components: region 1, fluid in the fill line, a 1-mm diameter, 6-mm long cylinder comprising 0.8% of the total fluid moment of inertia [solid (black) line], and region 2, fluid at the periphery of the cell, modeled as a cavity of height 28 μm [dashed (red) line] comprising 3.2% of the moment of inertia. The dash-dotted (green) line shows the sum of the contributions from the two bulk fluid components.

where β_1 contributes to the damping of the pendulum and β_2 to the moment of inertia. Temperature dependence of these values is determined by the temperature dependence of the viscosity of the fluid, $\eta(T)$.

Near T_c, we expect the normal state bulk viscosity to scale as T^{-2}. Above $T > 10$ mK the viscosity deviates from the Fermi liquid T^{-2} behavior and we use the following relations between the thermal conductivity (κ), heat capacity (C_V), and the viscosity (η) to calculate higher temperature values for η:

$$\kappa = \frac{1}{3}C_V v_F^2 \tau_\kappa, \qquad \text{(A3)}$$

$$\eta = \frac{1}{5}\frac{m^*}{m}\rho v_F^2 \tau_\eta, \qquad \text{(A4)}$$

$$C_V = m^*\frac{\pi^2 k_B}{\hbar^2}\left(\frac{V}{3\pi^2 N}\right)^{2/3} RT. \qquad \text{(A5)}$$
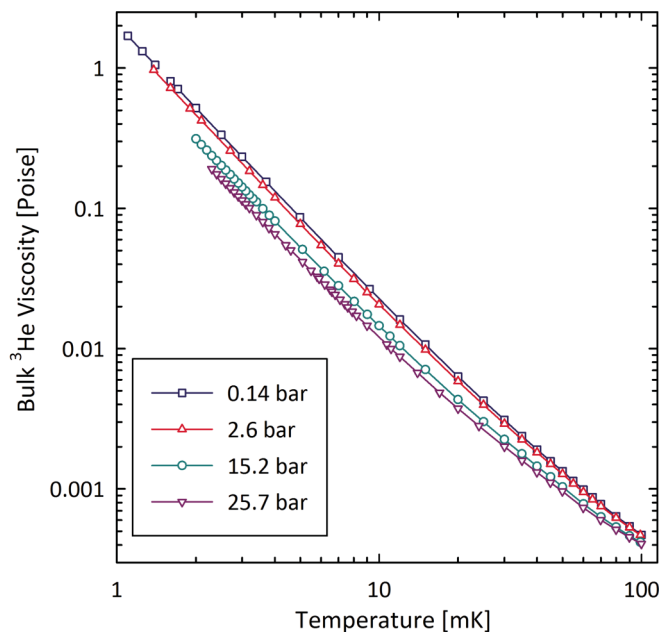
FIG. 8. (Color online) Values of viscosity in the normal state at the four experimental pressures.

Assuming that density and molar volume do not change in the temperature range 1–100 mK, and assuming $\tau_\eta \propto \tau_\kappa$, we can infer that $\eta \propto \kappa$. To find the exact values for the viscosity in the normal state, we use the values for $\eta(T_c)$ given in Refs. [65,66], and $\kappa(T_c)$ in Ref. [67] and divide the two values to find the proportionality factor. We then multiply $\kappa(T)$ from Ref. [67] by this factor for each of the pressures we are interested and we find $\eta(T)$ up to 100 mK. The values for the viscosity for the four experimental pressures we used to calculate bulk fluid contribution in the normal state are shown in Fig. 8. In the superfluid state, experimental values for the superfluid fraction are taken from Ref. [68] and for the viscosity from Ref. [38]

Numerically solving Eq. (A1), we can calculate the contribution from the bulk fluid in the fill line. This contribution is shown with a solid (black) line in Figs. 2 and 7. It is evident in Fig. 7 that there is bulk fluid within the cell we have not yet accounted for.

The steel cavity containing the aerogel was dry fitted in the epoxy cast to prevent epoxy running in. We believe this resulted in small pockets of bulk fluid existing around the periphery of the cell. While we cannot do an exact calculation for the effects of these regions the same way as we did for the fluid in the torsion rod, we can still use the uncoupled moment of inertia data (Fig. 7) to estimate the contribution to the pendulum's dissipation. We assume that the relationship between the real and the imaginary part of the torque arising from the cell periphery bulk fluid is the same as that of a uniform thickness film encompassing all of the cell. For a thin film of fluid with a thickness h and inertial contribution I_{per}, the torque exerted is $N = \beta_1 + i\omega\beta_2$, with

$$\beta_1 = \omega I_{per} \frac{\delta}{h} \frac{\sin(h/\delta) - \sinh(h/\delta)}{\cos(h/\delta) + \cosh(h/\delta)}, \tag{A6}$$

$$\beta_2 = I_{per} \frac{\delta}{h} \frac{\sin(h/\delta) + \sinh(h/\delta)}{\cos(h/\delta) + \cosh(h/\delta)}, \tag{A7}$$

where $\delta = \sqrt{2\eta/\rho\omega}$ is the viscous penetration depth of the fluid. Fitting to the dissipation data in Fig. 2, we find $h = 28\ \mu$m and $I_{per} = 0.032 I_f$, where I_f is the moment of inertia of all the helium in the torsion pendulum head. These values are consistent with our expectations. The accuracy to which the epoxy cast and stainless steel cell are machined is within one-thousand of an inch, i.e., 25 μm, and a film of that thickness around all of the cell surface amounts to $0.05 I_f$. Since the bulk fluid is more likely coming from a few separate regions around the periphery, rather than from a continuous film, we would expect that $I_{per} \lesssim 0.05 I_f$. We also use these values and the viscosity of ^{3}He to obtain the fraction of decoupled fluid from the periphery (region 2) which we plot as the dashed (red) line in Fig. 6.

At the lowest experimental pressures (0.14, 2.6, and 4 bar), the liquid in the aerogel does not transition to a superfluid state. At these pressures, the resonance period shift below T_c originates from the bulk fluid regions. In addition to the bulk fluid decoupling, we observe fourth sound resonance crossings effects, which occur at specific values of the sound velocity and therefore ρ_s/ρ^{bulk}. We obtain a good fit to these data using the model described in this appendix, which gives an independent confirmation that bulk fluid effects are fully accounted for. More information about these effects can be found in the supplementary material of Ref. [23].

APPENDIX B: DYNAMICS OF NORMAL ^{3}HE IN AEROGEL

We start by rewriting Eqs. (6) and (7) as

$$\frac{\partial^2 \Omega_a}{\partial z^2} + a_a \Omega_a - b_a \Omega_l = 0, \tag{B1}$$

$$\frac{\partial^2 \Omega_l}{\partial z^2} + a_l \Omega_l - b_l \Omega_a = 0, \tag{B2}$$

where we have defined the coefficients a and b as

$$a_a = i\frac{\rho\omega}{\mu} \quad b_a = a_a \left(1 - i\omega\tau_F \frac{\rho_a}{\rho}\right), \tag{B3}$$

$$a_l = -\frac{\rho}{\eta\tau_F}, \quad b_l = a_l (1 - i\omega\tau_F). \tag{B4}$$

Solving the coupled differential equations, we arrive at

$$\Omega_a(z) = \left[\frac{D - \frac{a_l - a_a}{2} - b_a}{2D} \frac{\cos(k_1 z)}{\cos(k_1 h/2)}\right.$$
$$\left. + \frac{D + \frac{a_l - a_a}{2} + b_a}{2D} \frac{\cos(k_2 z)}{\cos(k_2 h/2)}\right]\dot\theta, \tag{B5}$$

$$\Omega_l(z) = \left[\frac{D - \frac{a_a - a_l}{2} - b_l}{2D} \frac{\cos(k_1 z)}{\cos(k_1 h/2)}\right.$$
$$\left. + \frac{D + \frac{a_a - a_l}{2} + b_l}{2D} \frac{\cos(k_2 z)}{\cos(k_2 h/2)}\right]\dot\theta, \tag{B6}$$

where $D = \sqrt{(\frac{a_l - a_a}{2})^2 + b_l b_a}$ and $k_{1,2} = \sqrt{\frac{a_l + a_a}{2} \pm D}$.

To obtain a qualitative picture of the angular velocity profiles, we can explore the fact that $\omega\tau_f \ll 1$ and $\eta\omega/\mu \ll 1$. The coefficients $(D \pm \frac{a_l - a_a}{2} \pm b_{a,l})/2D$ and the values of $k_{1,2}$ in Eqs. (B5) and (B6) are approximated to the lowest order.

This approximation gives us the z dependence of the angular velocity of the aerogel, $\Omega_a(z)$, and that of the fluid $\Omega_l(z)$:

$$\Omega_a(z) \approx \dot{\theta} \frac{\cos\left[\sqrt{\frac{(\rho+\rho_a)\omega^2}{\mu}} z\right]}{\cos\left[\sqrt{\frac{(\rho+\rho_a)\omega^2}{\mu}} \frac{h}{2}\right]}, \tag{B7}$$

$$\Omega_l(z) \approx \dot{\theta} \left\{ \frac{\cos\left[\sqrt{\frac{(\rho+\rho_a)\omega^2}{\mu}} z\right]}{\cos\left[\sqrt{\frac{(\rho+\rho_a)\omega^2}{\mu}} \frac{h}{2}\right]} - i\omega\tau_f \frac{\cosh\left[\frac{z}{\delta_d}\right]}{\cosh\left[\frac{h}{2\delta_d}\right]} \right\}, \tag{B8}$$

where $\delta_d = \sqrt{\eta\tau_f/\rho} \ll h$ is the "dirty" fluid penetration depth, i.e., the length scale over which the velocity of the helium fluid deviates from the Drude flow regime with respect to the aerogel velocity. We observe that the shape of both aerogel and fluid velocity profiles is largely set by the elastic modulus of the aerogel, μ. The relative velocity difference between the aerogel and the helium fluid is of the order of $\omega\tau_f \ll 1$ of the total velocity.

Equations (B7) and (B8) present a qualitative picture for the differences in the velocities of the flow and the aerogel, but we need to include higher-order terms in the expressions above to estimate the dissipation factors associated with the aerogel and the fluid in the cell. Importantly, we also allow the possibility of the elastic modulus of the aerogel to be a complex number, $\mu = \mu_{\rm re} - i\mu_{\rm im}$, with $\mu_{\rm im}/\mu_{\rm re} \ll 1$. Then for $k_{1,2}$ we have

$$k_1 \approx \sqrt{\frac{(\rho+\rho_a)\omega^2}{\mu_{\rm re}}}$$
$$\times \left\{ 1 + i \left[\frac{\omega\eta}{2\mu_{\rm re}} + \frac{\mu_{\rm im}}{\mu_{\rm re}} + \frac{\omega\tau_f}{2} \frac{\rho}{(\rho+\rho_a)} \right] \right\}, \tag{B9}$$

$$k_2 \approx \frac{i}{\delta_d}\left[1 - i\left(\frac{\omega\eta}{2\mu_{\rm re}} + \frac{\omega\tau_f}{2}\right)\right]. \tag{B10}$$

As for the coefficients in Eqs. (B5) and (B6):

$$C_1 = \frac{D - \frac{a_l-a_a}{2} - b_a}{2D} \approx 1, \tag{B11}$$

$$C_2 = \frac{D + \frac{a_l-a_a}{2} + b_a}{2D} \approx (\omega\tau_f)\left(\frac{\eta\omega}{\mu_{\rm re}}\right), \tag{B12}$$

$$C_3 = \frac{D - \frac{a_a-a_l}{2} - b_l}{2D} \approx 1 + i\omega\tau_f, \tag{B13}$$

$$C_4 = \frac{D + \frac{a_a-a_l}{2} + b_l}{2D} \approx -i\omega\tau_f\left(1 + i\frac{\eta\omega}{\mu_{\rm re}}\frac{\rho+\rho_a}{\rho}\right). \tag{B14}$$

The expressions for the induced torque by the aerogel (N_a) and the helium liquid (N_l) can be written as

$$N_a = i\omega I_a \frac{2\mu}{\rho_a\omega^2 h}\left[C_1 k_1 \tan\left(k_1\frac{h}{2}\right) + C_2 k_2 \tan\left(k_2\frac{h}{2}\right)\right]\dot{\theta}, \tag{B15}$$

$$N_l = I_l \frac{2\eta}{\rho h}\left[C_3 k_1 \tan\left(k_1\frac{h}{2}\right) + C_4 k_2 \tan\left(k_2\frac{h}{2}\right)\right]\dot{\theta}. \tag{B16}$$

Further, the expressions for the tangents can be approximated as

$$\tan\left(k_1\frac{h}{2}\right) \approx k_1\frac{h}{2} + \frac{\left(\frac{(\rho+\rho_a)\omega^2 h}{4\mu_{\rm re}}\right)^{3/2}}{3 - \left(\frac{(\rho+\rho_a)\omega^2 h}{4\mu_{\rm re}}\right)} + i\frac{\left[\frac{(\rho+\rho_a)\omega^2 h}{4\mu_{\rm re}}\right]^{3/2}}{1 - \left[\frac{(\rho+\rho_a)\omega^2 h}{4\mu_{\rm re}}\right]}$$
$$\times \left(\frac{\eta\omega}{\mu_{\rm re}} + \frac{\mu_{\rm im}}{\mu_{\rm re}}\frac{\omega\tau_f}{2}\frac{\rho}{\rho+\rho_a}\right), \tag{B17}$$

$$\tan\left(k_2\frac{h}{2}\right) \approx i, \tag{B18}$$

where we used the following relation:

$$\tan(\alpha + i\beta) \approx \alpha\left(1 + \frac{\alpha^2}{3 - 3\alpha^2}\right) + i\beta\left(\frac{\alpha^2}{1 - \alpha^2}\right), \tag{B19}$$

which is true in the case of $\beta \ll \alpha$ and $\alpha \lesssim 0.1$. For the expression for $\tan(k_2h/2)$, we use the fact that $|k_2h/2| \sim h/\delta_d \gg 1$ and that ${\rm Im}(k_2h/2) \gg {\rm Re}(k_2h/2)$.

Putting all of these expressions together, we arrive at

$$N_{\rm ind} = N_a + N_l$$
$$\approx -\left[(I_a+I_l)\omega\frac{\xi}{3-\xi}\left(\frac{\eta\omega}{\mu_{\rm re}}+\frac{\mu_{\rm im}}{\mu_{\rm re}}\right) + I_l\omega^2\tau_f\frac{3-\xi}{3-3\xi}\right]\dot{\theta}$$
$$+ i\omega\frac{3-2\xi}{3-3\xi}(I_a+I_l)\dot{\theta}, \tag{B20}$$

where $\xi = \frac{(\rho+\rho_a)\omega^2 h^2}{4\mu_{\rm re}}$ and we have ignored terms containing $\delta_d/h \ll 1$. We can simplify further, since $\xi \sim 10^{-2}$:

$$N_{\rm ind} \approx -\left[(I_a+I_l)\frac{(\rho+\rho_a)\omega^4 h^2}{12\mu_{\rm re}^2}\left(\eta+\frac{\mu_{\rm im}}{\omega}\right) + I_l\omega^2\tau_f\right]\dot{\theta}$$
$$+ i\omega(I_a+I_l)\dot{\theta}. \tag{B21}$$

Using this expression for the induced torque, we arrive at the expression for Q^{-1} in Eq. (8).

[1] E. R. Ulm, J.-T. Kim, T. R. Lemberger, S. R. Foltyn, and X. Wu, Phys. Rev. B **51**, 9193 (1995).

[2] D. N. Basov, A. V. Puchkov, R. A. Hughes, T. Strach, J. Preston, T. Timusk, D. A. Bonn, R. Liang, and W. N. Hardy, Phys. Rev. B **49**, 12165 (1994).

[3] C. Bernhard, J. L. Tallon, C. Bucci, R. De Renzi, G. Guidi, G. V. M. Williams, and Ch. Niedermayer, Phys. Rev. Lett. **77**, 2304 (1996).

[4] K. Fujita, T. Noda, K. M. Kojima, H. Eisaki, and S. Uchida, Phys. Rev. Lett. **95**, 097006 (2005).

[5] S. Graser, P. J. Hirschfeld, L.-Y. Zhu, and T. Dahm, Phys. Rev. B **76**, 054516 (2007).

[6] S. Sanna, F. Coneri, A. Rigoldi, G. Concas, S. R. Giblin, and R. De Renzi, Phys. Rev. B **82**, 100503(R) (2010).

[7] E. V. Thuneberg, S. K. Yip, M. Fogelström, and J. A. Sauls, Phys. Rev. Lett. **80**, 2861 (1998).

[8] R. Hänninen and E. V. Thuneberg, Phys. Rev. B **67**, 214507 (2003).

[9] P. Sharma and J. A. Sauls, Physica B **329**, 313 (2003).

[10] D. Einzel and J. M. Parpia, Phys. Rev. Lett. **81**, 3896 (1998).

[11] J. V. Porto and J. M. Parpia, Phys. Rev. Lett. **74**, 4667 (1995).

[12] D. T. Sprague, T. M. Haard, J. B. Kycia, M. R. Rand, Y. Lee, P. J. Hamot, and W. P. Halperin, Phys. Rev. Lett. **75**, 661 (1995).

[13] J. A. Sauls, Yu. M. Bunkov, E. Collin, H. Godfrin, and P. Sharma, Phys. Rev. B **72**, 024507 (2005).

[14] H. Götz and G. Eska, Physica B **329**, 307 (2003).

[15] P. A. Reeves, G. Tvalashvili, S. N. Fisher, A. M. Guénault, and G. R. Pickett, J. Low Temp. Phys. **129**, 185 (2002).

[16] P. Venkataramani and J. A. Sauls, Physica B **284**, 297 (2000).

[17] H. Takeuchi, S. Higashitani, K. Nagai, H. C. Choi, B. H. Moon, N. Masuhara, M. W. Meisel, Y. Lee, and N. Mulders, Phys. Rev. Lett. **108**, 225307 (2012).

[18] Y. Nagato, M. Yamamoto, and K. Nagai, J. Low Temp. Phys. **110**, 1135 (1998).

[19] A. B. Vorontsov and J. A. Sauls, Phys. Rev. B **68**, 064508 (2003).

[20] Y. Tsutsumi, M. Ichioka, and K. Machida, Phys. Rev. B **83**, 094510 (2011).

[21] S. N. Fisher, A. M. Guénault, N. Mulders, and G. R. Pickett, Phys. Rev. Lett. **91**, 105303 (2003).

[22] H. Choi, K. Yawata, T. M. Haard, J. P. Davis, G. Gervais, N. Mulders, P. Sharma, J. A. Sauls, and W. P. Halperin, Phys. Rev. Lett. **93**, 145301 (2004).

[23] R. G. Bennett, N. Zhelev, E. N. Smith, J. Pollanen, W. P. Halperin, and J. M. Parpia, Phys. Rev. Lett. **107**, 235504 (2011).

[24] K. Aoyama and R. Ikeda, Phys. Rev. B **73**, 060504 (2006).

[25] G. E. Volovik, J. Low Temp. Phys. **150**, 453 (2008).

[26] J. I. A. Li, A. M. Zimmerman, J. Pollanen, C. A. Collett, W. J. Gannon, and W. P. Halperin, arXiv:1401.5153 [cond-mat.supr-con].

[27] J. A. Sauls, Phys. Rev. B **88**, 214503 (2013).

[28] R. Combescot, J. Low Temp. Phys. **18**, 537 (1975).

[29] J. E. Berthold, R. W. Giannetta, E. N. Smith, and J. D. Reppy, Phys. Rev. Lett. **37**, 1138 (1976).

[30] J. Pollanen, K. R. Shirer, S. Blinstein, J. P. Davis, H. Choi, T. M. Lippman, W. P. Halperin, and L. B. Lurio, J. Non-Cryst. Solids **354**, 4668 (2008).

[31] R. G. Bennett, N. Zhelev, A. D. Fefferman, K. Y. Fang, J. Pollanen, P. Sharma, W. P. Halperin, and J. M. Parpia, J. Low Temp. Phys. **162**, 174 (2011).

[32] E. Nazaretski, S. Dimov, R. O. Pohl, and J. M. Parpia, J. Low Temp. Phys. **138**, 881 (2005).

[33] A. Golov, D. A. Geller, J. M. Parpia, and N. Mulders, Phys. Rev. Lett. **82**, 3492 (1999).

[34] E. Nazaretski, N. Mulders, and J. M. Parpia, JETP Lett. **79**, 383 (2004).

[35] M. J. McKenna, T. Slawecki, and J. D. Maynard, Phys. Rev. Lett. **66**, 1878 (1991).

[36] N. Mulders, R. Mehrotra, L. S. Goldner, and G. Ahlers, Phys. Rev. Lett. **67**, 695 (1991).

[37] H. Alles, J. J. Kaplinsky, P. S. Wootton, J. D. Reppy, and J. R. Hook, Physica B **255**, 1 (1998).

[38] D. Einzel and J. M. Parpia, Phys. Rev. Lett. **58**, 1937 (1987).

[39] A. I. Golov, D. Einzel, G. Lawes, K. Matsumoto, and J. M. Parpia, Phys. Rev. Lett. **92**, 195301 (2004).

[40] Y. Nago, K. Obara, R. Kado, H. Yano, O. Ishikawa, and T. Hata, J. Low Temp. Phys. **148**, 597 (2007).

[41] K. Obara, C. Kato, T. Matsukura, Y. Nago, R. Kado, H. Yano, O. Ishikawa, T. Hata, S. Higashitani, and K. Nagai, Phys. Rev. B **82**, 054521 (2010).

[42] S. Higashitani, J. Low Temp. Phy. **114**, 161 (1999).

[43] S. Higashitani, M. Miura, T. Ichikawa, M. Yamamoto, and K. Nagai, Phys. Rev. Lett. **89**, 215301 (2002).

[44] S. Higashitani, M. Miura, M. Yamamoto, and K. Nagai, Phys. Rev. B **71**, 134508 (2005).

[45] S. Higashitani, T. Ichikawa, M. Yamamoto, M. Miura, and K. Nagai, Physica B **329**, 299 (2003).

[46] A. A. Abrikosov and L. P. Gorkov, Sov. Phys. JETP **12**, 1243 (1961).

[47] W. P. Halperin, H. Choi, J. P. Davis, and J. Pollanen, J. Phys. Soc. Jpn. **77**, 111002 (2008).

[48] J. A. Sauls and P. Sharma, Phys. Rev. B **68**, 224502 (2003).

[49] P. Sharma and J. A. Sauls, J. Low Temp. Phys. **125**, 115 (2001).

[50] A. M. Zimmerman, M. G. Specht, D. Ginzburg, J. Pollanen, J. I. A. Li, C. A. Collett, W. J. Gannon, and W. P. Halperin, J. Low Temp. Phys. **171**, 745 (2013).

[51] T. E. Gomez Alvarez-Arenas, F. R. Montero de Espinosa, M. Moner-Girona, E. Rodriguez, A. Roig, and E. Molins, Appl. Phys. Lett. **81**, 1198 (2002).

[52] A. Zimmerman, J. Gross, and J. Fricke, J. Non-Cryst. Solids **186**, 238 (1995).

[53] T. Schlief, J. Gross, and J. Fricke, J. Non-Cryst. Solids **145**, 223 (1992).

[54] J. V. Porto and J. M. Parpia, Phys. Rev. B **59**, 14583 (1999).

[55] H. C. Choi, N. Masuhara, B. H. Moon, P. Bhupathi, M. W. Meisel, Y. Lee, N. Mulders, S. Higashitani, M. Miura, and K. Nagai, Phys. Rev. Lett. **98**, 225301 (2007).

[56] N. B. Kopnin, Physica B **210**, 267 (1995).

[57] T. D. C. Bevan, A. J. Manninen, J. B. Cook, H. Alles, J. R. Hook, and H. E. Hall, J. Low Temp. Phys. **109**, 423 (1997).

[58] H. E. Hall, P. L. Gammel, and J. D. Reppy, Phys. Rev. Lett **52**, 1701 (1984).

[59] S. N. Fisher, A. M. Guénault, C. J. Kennedy, and G. R. Pickett, Phys. Rev. Lett. **63**, 2566 (1989).

[60] D. I. Bradley, S. N. Fisher, A. M. Guénault, R. P. Haley, N. Mulders, S. O'Sullivan, G. R. Pickett, J. Roberts, and V. Tsepelin, Phys. Rev. Lett. **98**, 075302 (2007).

[61] M. C. Cross and P. W. Anderson, *Proceedings of the 14th International Conference on Low Temperature Physics* (North-Holland, Amsterdam, 1975), Vol. 1, p. 29.

[62] M. C. Cross, AIP Conf. Proc. **103**, 325 (1983).

[63] D. I. Bradley, S. N. Fisher, A. M. Guénault, R. P. Haley, G. R. Pickett, J. E. Roberts, S. O'Sullivan, and V. Tsepelin, J. Low Temp. Phys. **150**, 445 (2008).

[64] J. M. Parpia and J. D. Reppy, Phys. Rev. Lett. **43**, 1332 (1979).

[65] C. N. Archie, T. A. Alvesalo, J. D. Reppy, and R. C. Richardson, J. Low Temp. Phys. **42**, 295 (1981).

[66] J. M. Parpia, D. J. Sandiford, J. E. Berthold, and J. D. Reppy, Phys. Rev. Lett. **40**, 565 (1978).

[67] D. S. Greywall, Phys. Rev. B **29**, 4933 (1984).

[68] J. M. Parpia, D. G. Wildes, J. Saunders, E. K. Zeise, J. D. Reppy, and R. C. Richardson, J. Low Temp. Phys. **61**, 337 (1985).